NJC

Accepted Manuscript

This is an *Accepted Manuscript*, which has been through the Royal Society of Chemistry peer review process and has been accepted for publication.

Accepted Manuscripts are published online shortly after acceptance, before technical editing, formatting and proof reading. Using this free service, authors can make their results available to the community, in citable form, before we publish the edited article. We will replace this *Accepted Manuscript* with the edited and formatted *Advance Article* as soon as it is available.

You can find more information about *Accepted Manuscripts* in the **Information for Authors**.

Journal Name

ARTICLE

Synthesis of Pt and bimetallic PtPd nanostructures on Au nanoparticles for use as methanol tolerant oxygen reduction reaction catalysts

In-Su Park[a,†], Ok-Hee Kim[b,†], Jung Won Kim[c], Baeck Choi[d], Yong-Hun Cho[c,*] and Yung-Eun Sung[d,e*]

Core-shell structured Au-PtPd/C and Au-Pt/C nanoparticle (NP) was prepared usinga successive reduction process on carbon supported Au with PtPd and Pt particles. Structural analyses of the core-shell NPs revealed uniformly distributed fine particles (< 5 nm in diameter) on carbon particle, and selectively deposited Pt and bimetallic PtPd structures on the Au surface. The activity of NP was investigated for oxygen reduction reaction (ORR) in both H_2SO_4 solutions with and without CH_3OH. In Au-Pt and Au-PtPd NPs, the activities for ORR decreased in solution without CH_3OH as the Pd amount increased while Au-PtPd NPs showed higher activity than Au-Pt NPs in solution with CH_3OH due to its enhanced tolerance for methanol oxidation. That is, the high methanol oxidation reaction tolerance of Au-PtPd NPs is ascribed to the synergistic effect resulting from its thin structure and bimetallic PtPd composition.

Introduction

One of the main obstacles for the commercialization of direct methanol fuel cells (DMFCs) is the methanol crossover from the anode to the cathode through the polymer electrolyte during the cell operation. Also, a competitive reaction between oxygen reduction reaction (ORR) and methanol oxidation reaction (MOR) in the cathode of DMFC produces a potential loss of 0.1 V and a 25 % reduction in efficiency.[1] To overcome these difficulties, there have been two main tries over the last few decades, for achieving higher catalytic activity for the ORR, and more selective activation to methanol oxidation. These goals have been mainly obtained by the modification of the structure and composition of the catalyst, which are major features in determining the adsorption/desorption of reactants and catalytic properties for an electrochemical reaction.[2] Platinum (Pt) demonstrate the high reactivity to MOR, however, pure Pt is easily poisoned by carbon monoxide (CO), which is the main intermediate species formed during the MOR. So, the pure Pt has low catalytic stability as an electro-catalytic material on the anode of DMFCs.[3] Therefore Pt based bimetallic nanoparticles, such as

PtRu, PtSn and PtMo are generally employed to avoid the formation of CO on Pt sites.[4-5] In particular. It is well known that PtPd bimetallic nanoparticles (NPs) as a cathode catalysts exhibit an improved performance in DMFCs and a high tolerance for CO adsorption, and theoretical density functional theory (DFT) studies have shown that the presence of Pd atoms facilitates the dissociation of O_2 on Pt.[5] Generally, the activity enhancement of Pd-based alloy catalysts for the ORR can be related to the changes in structural parameters. Therefore, it can be concluded that the design of bimetallic PtPd structures on a nanometer scale is valuable for enhancing the MOR tolerance in the cathode of DMFC.

In our prior studies, carbon-supported Au NPs (Au/C, ca. 4 nm in diameter) decorated with Pt, Pd and PtRu were prepared using a successive reduction process, and these NPs exhibited high electrocatalytic reactivity in methanol and formic acid oxidation reactions, due to their high utilization and the modified intrinsic properties of active elements by Au NPs.[6-9]

In line with our ongoing effort to investigate the reactivity of surface-modified Au NPs, we have attempted to synthesize bimetallic PtPd-modified Au (Au-PtPd; core-shell structure) NPs and characterize their reactivity for ORR in solutions with and without CH_3OH. Here, we report electrochemical evidence representing the synergistic effect of Au-PtPd NPs in electrocatalytic reactivity.

Results and discussion

[a.] Mineral Resources Research Division, Korea Institute of Geoscience and Mineral Resources, Yuseong-Gu, Daejeon 305-350, Republic of Korea
[b.] Department of Science, Republic of Korea Naval Academy, Jinhae-gu, Changwon 646-797, South Korea
[c.] Department of Chemical Engineering, Kangwon National University, Samcheok 245-711, South Korea
[d.] Center for Nanoparticle Research, Institute for Basic Science (IBS), Seoul 151-742, South Korea
[e.] School of Chemical and Biological Engineering, Seoul National University (SNU), Seoul 151-744, South Korea.
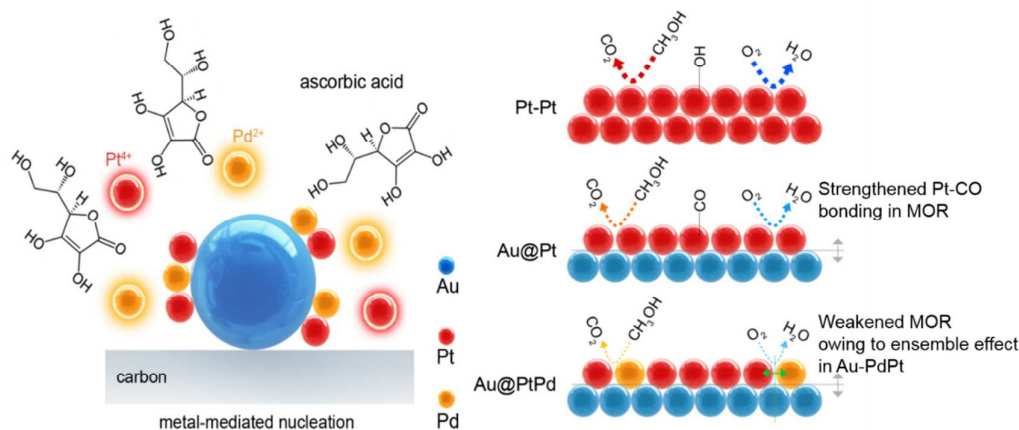† These authors contributed equally to this work.
* Corresponding authors

Fig. 1 shows that the schematic diagram of the fabrication   adsorption and these two adjacent Pt sites are abundantly

Fig. 1 Schematic diagram of the fabrication process of Au-PtPd core-shell structure NPs (left) and conceptual diagram of the Pt/C, Au-Pt/C and Au-PtPd/C cathode surface during the methanol oxidation and oxygen reduction (right).

process of Au-PtPd core-shell structure NPs. The Au-PtPd NPs were designated as Au-PtPdX, where X indicates the atomic ratio of Pt to Pd. The prepared Au-PtPd/C catalyst was characterized by high-resolution transmission electron microscopy (HR-TEM) to investigate the size and dispersion of the NPs (Fig. 2). Au/C NPs was first prepared, because they have been one of the basic seed materials for the seed-mediated preparation of multi-metallic nanoparticles because of their easy preparation in various sizes and shapes.[10] Next, selective deposition reaction of Pt, PtPd and Pd on Au/C NP was carried out. Generally, NP morphology is mainly determined by the shape of the seeds, the direction of growth, and the growth rate. Reducing power is one of main factor for control the shape of NPs. Thus for core/shell structure, the first reducing agent for Au/C particle was $NaBH_4$, which is frequently used to prepare high-surface-area precious metal-based alloy electrocatalysts.[11-12] Then, milder reducing agent, ascorbic acid was added to the Au/C-dispersed solution at room temperature for selective deposition of Pt, PtPd and Pd on Au/C particle.

The reducing power can be varied by using different reducing agents such as $NaBH_4$, ascorbic acid, diols, or citric acid.[13-14] Moreover, altering the pH value or reaction temperature can also modulate the reducing power of a given reducing agent. The rates and direction of crystal growth can be controlled by the addition of various reducing agents, surface-capping agents, absorptive small molecules, or inorganic ions. The reaction temperature and precursor concentration often play an important role in controlling the final shape of NPs.[15]

Bimetallic PtPd-modified Au/C NP is very interesting as an object of MOR catalyst. Theoretically, for methanol oxidation, the structure and composition of the catalyst requires a minimum of three active Pt sites nearby. Nevertheless, in the existence of both Pd on the catalyst surface, methanol adsorption on the catalyst surface is unlikely in most cases because there are not an enough number of active Pt sites nearby on the surface of the Au-PtPd alloy system. Yet, the ORR activity of the Pt alloy catalyst is not seriously delayed by such alloying. As only two Pt sites are required for oxygen

Fig. 2 HR-TEM images and particle size distribution histogram of Au-PtPd1.0 and Pt-C catalysts: (a) Au-PtPd1.0 at low magnification, (b) enlarged image of box in (a), inset of (b) is particle size distribution histogram of Au-PtPd1.0. (c) HR-TEM image of Pt-C catalyst (inset of c: closer look of dendritic Pt).
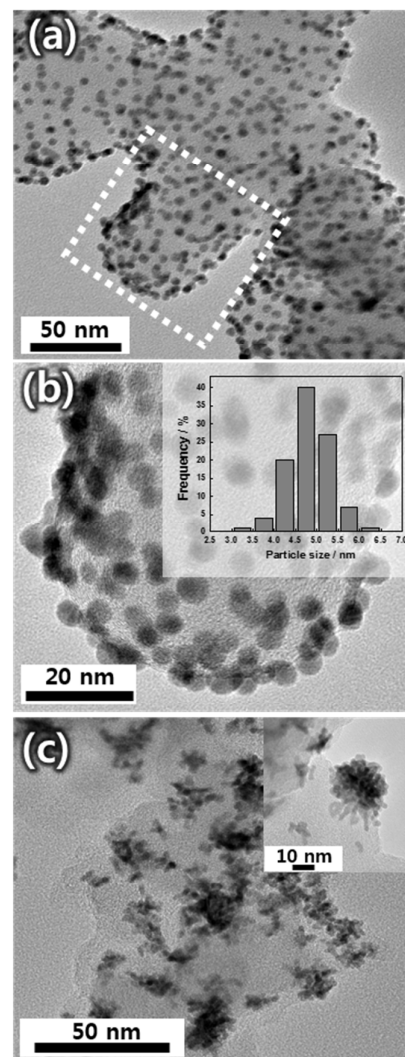
available on the surface of the alloy,[15–21] Pd in the Au-PtPd/C catalysts play an important role in the inactivation of methanol adsorption and oxidation at the cathode. These conceptions for methanol tolerance and ORR activities of Au-PtPd/C catalysts are well symbolized in conceptual diagrams at the right of Fig. 1. For a bimetallic catalyst system, this phenomenon is well known as 'ensemble effect', which occurs when the active component is diluted by catalytically inert metals forming a bimetallic catalyst that causes changes in the distribution of active sites and opens different reaction pathways.[22] Therefore, the effects of Pt and Pd in the Au-PtPd/C catalyst may be responsible for the enhanced MOR tolerance.

In Fig. 2a and b, HR-TEM images of Au-PtPd NPs show the uniformly dispersed NPs on carbon particles of a round shape, and with a surface particle density similar to that of Au/C. As shown in the inset of Fig. 2b, the particle size distribution and mean particle size were obtained from the magnified image with the assumption of spherical NPs. The obtained particle size (4.82 nm) of Au-PtPd1.0 NPs was larger than 3.48 nm of Au/C and close to that (4.55 nm) of Au-Pt NPs, indicating the thickness of 0.67 nm (c.a. 1.9 atomic layer) in PtPd structure. For validating a role of Au NPs, Pt NPs (Pt-C) were synthesized by the same process with Au-Pt NPs using blank carbon particles instead of Au/C. Fig. 2c shows the aggregated Pt structure (dendritic growth) indicating Pt growth by the autocatalytic process of ascorbic acid.

Also XRD profile in Fig. 3 represents the main peaks of pure Au NPs representing the PtPd structure in a small cluster or thin layer on Au NPs. Four major peaks at38.1, 44.3, 64.5, and 77.4° in the spectrum correspond to Au(111), (200), (220) and (311) planes, respectively. Therefore, these results of TEM and XRD represent the selective deposition of Pt and Pd atoms on Au NPs under the optimized reduction conditions.

Fig. 4a shows the XPS spectrum of Au-Pt, Au-PtPd, Au-Pd NPs, calibrated after fitting Au $4f_{7/2}$ (84.0 eV). The constant intensities of Au $4f$ signals were observed while Pt $4f$ and Pd $3d$ were systematically dependent on the atomic ratio between Pt and Pd. In other words, an increase in intensity of Pt signals

with an increase in atomic percentage (at. %) of Pt resulted in the decreased intensity for Pd signal. As shown in Fig. 4b, the peak position of Pt $4f_{7/2}$ shifted slightly to lower binding energy as the could be associated with the change in Pt oxidation states, metal–metal interaction, Pt–carbon interactions, or small cluster-size effects.[23] However, the metal–metal interaction mechanism is the only plausible reason for the peak shift of Pt atomic percentage of Pt increased in Au-PtPd NPs. Such shifts could be associated with the change in Pt

Fig. 4 (a) XPS spectrum of Au-Pt, Au-PtPd and Au-Pd NPs, and (b) the fitted Pt4*f* peaks of Au-Pt, Au-PtPdNPs, and (c) Binding energy of Pt $4f_{7/2}$ vs. atomic percentage of Pt curve. The atomic percentage (at. %) of Pt indicates that in total metals.
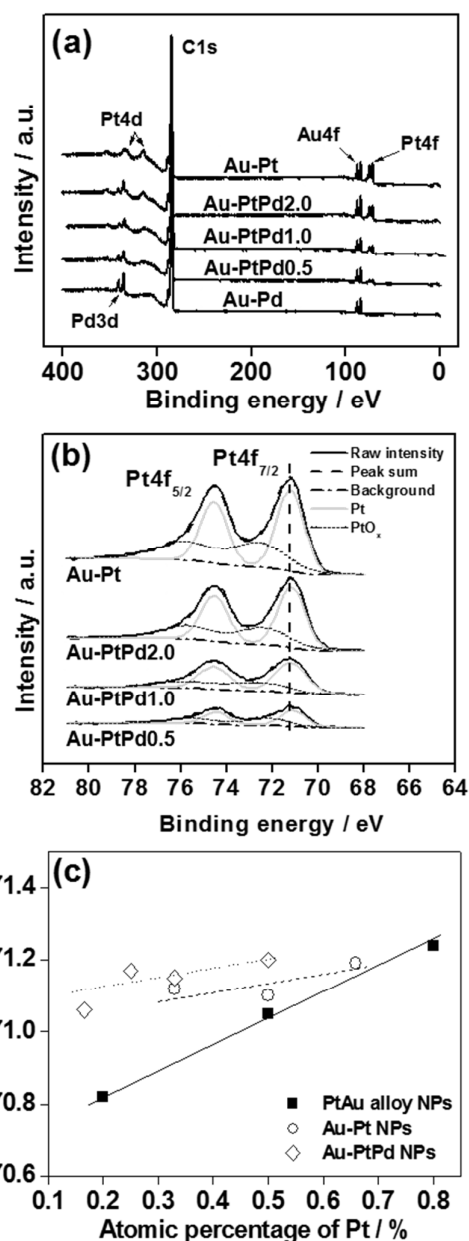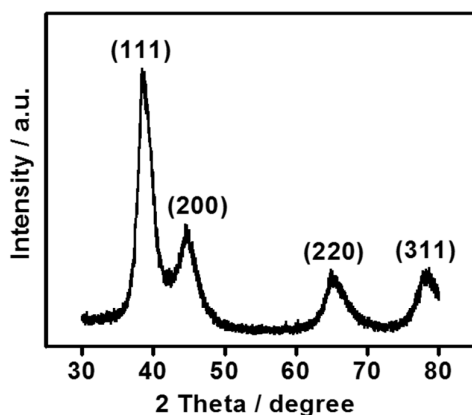

Fig. 3 XRD profile of Au-PtPd1.0 catalyst. XRD profile shows the main peaks of Au NPs.

ARTICLE

oxidation states, metal–metal interaction, Pt–carbon interactions, or small cluster-size effects.[23] However, the metal–metal interaction mechanism is the only plausible reason for the peak shift of Pt $4f_{7/2}$, given that the Pt oxidation states between the catalysts are similar and the unlikelihood of Pd in fluencing the Pt–carbon interactions. This should also indicate change in the electronic structure of Pt when it is alloyed with Pd. For the identification of Pt structure, the peak positions of $4f_{7/2}$ in Au-PtPd NPs were compared with those in Au-Pt NPs and PtAu alloy NPs. As shown in Fig. 4c, Pt structures in Au-Pt NPs and Au-PtPd NPs showed a different behavior to PtAu alloy NPs, and a higher binding energy than those of PtAu alloy NPs. Also, Au-PtPd NPs showed the slight higher binding energy than Au-Pt NPs. This result indicates a mainly non-alloyed Pt structure with Au elements and a bimetallic structure between Pt and Pd atoms.

Fig. 5a indicates the polarization curves of Pt/C (Johnson Matthey Co.) and Au-Pt NPs, and the currents were normalized by the geometric area of the glassy carbon (GC) electrode. The two samples represented similar activity in 0.5 M H_2SO_4 and no CH_3OH solution. However, under 0.5 M H_2SO_4/0.1 M CH_3OH solution, the rapid increase of oxidation currents started at 0.86V for Pt/C, and at 0.80 V for Au-Pt NPs, until a broad peak was obtained. Oxidation currents then decreased until 0.4 V. Interestingly, the peak current density (8 mA cm^{-2} @ 0.68 V) of oxidation peak for Au-Pt NPs was much lower than that (21 mA cm^{-2} @ 0.70 V) of Pt/C, indicating the higher methanol tolerance of the Pt structure on Au NPs. The high MOR tolerance of Au-Pt NPs might be due to the modified adsorbates-adsorption properties of the Pt overlayer on Au NPs.[23] Fig. 5b shows the polarization curves of Au-PtPd NPs, as compared with those of Au-Pt NPs. Fig. 5c and 5d shows the current densities at 0.8 V without (c) and with (d) 0.1M CH_3OH versus atomic percentage of Pt (%).The Au-PtPd NPs demonstrated a lower activity than Au-Pt NPs and Pt/C for ORR in 0.5 M H_2SO_4 solution, and the activities decreased with increasing Pd content. However, the Au-PtPd2.0 NPs represented a much higher activity than Pt/C in the 0.5 M H_2SO_4/0.1 M CH_3OH solution. Moreover, the Au-PtPd2.0 NPs contains about 2.5-times less amount of Pt than Pt/C. However, the Au-PtPd2.0 NPs represented a much higher activity than Au-Pt NPs in the 0.5 M H_2SO_4/0.1 M CH_3OH solution.

For the quantitative characterization of methanol tolerance in this study, a MOR tolerance coefficient (δ) was defined:

$$\delta = j_0/(j_0 - j_M)$$

where j_O and j_M are current densities at 0.8 V for ORR in 0.5 M H_2SO_4 and 0.5 M H_2SO_4/0.1 M CH_3OH solutions, respectively. As shown in Fig. 6, the MOR tolerance of Au-PtPd NPs increased as the ratio of Pt decreased, and represented much higher values than those of Au-Pt NPs and Pt/C. These results demonstrate clearly the high reactivity of Au-PtPd NPs for ORR in 0.5 M H_2SO_4/0.1 M CH_3OH solution, which is ascribed to the synergistic effect of the thin Pt structure and the bimetallic PtPd composition (at the right of Fig. 1).
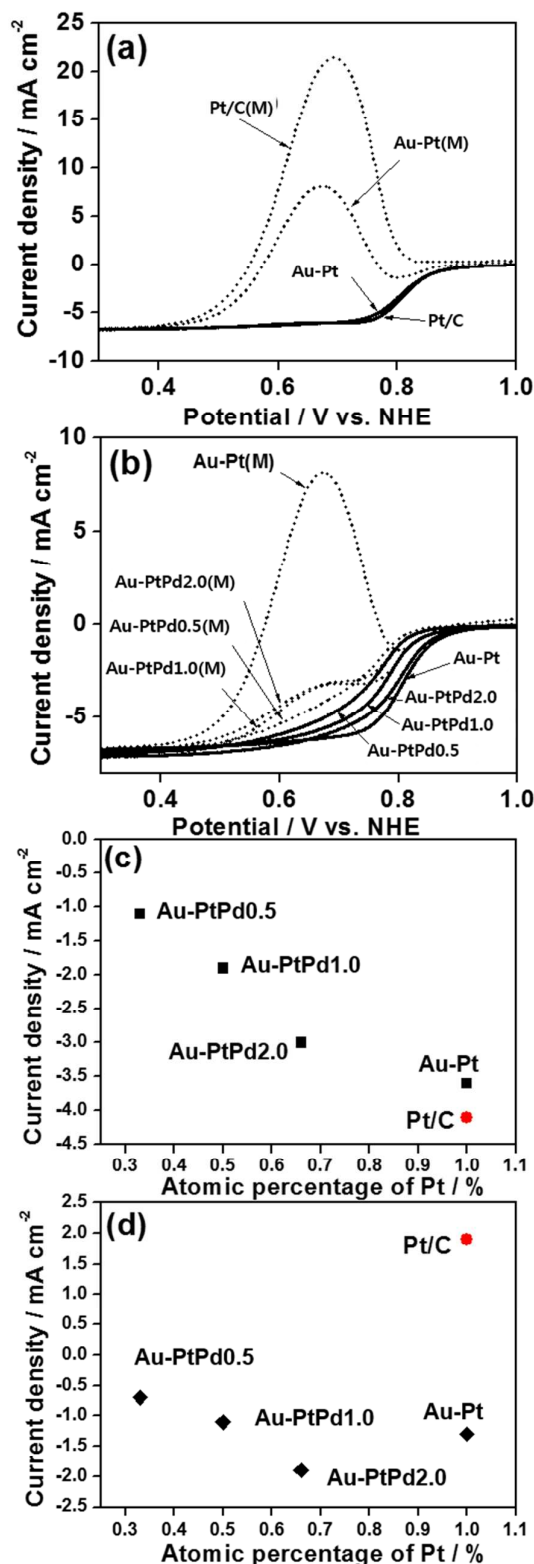

Fig. 5 Polarization curve of ORR for (a) Pt/C and Au-Pt NPs, (b) Au-Pt and Au-PtPd NPs, and current densities at 0.8 V vs. atomic percentage of Pt curve in 0.5M H_2SO_4 solution without (c) and with (d) 0.1M CH_3OH. The (M) indicates the measured CVs in 0.5 M H_2SO_4/0.1 M CH_3OH solution and the atomic percentage (at. %) of Pt indicates that in active metals.
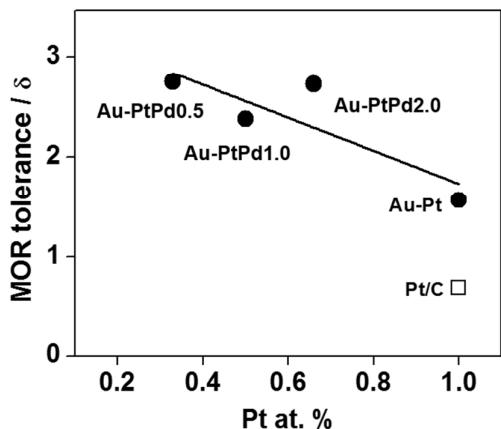
Fig. 6 MOR tolerance (δ) vs. atomic percentage of Pt curve. The atomic percentage (at. %) of Pt indicates that in active metals.

A CO-stripping analysis was performed to investigate the tolerance of Au-PtPd catalyst for MOR (Fig. 7). The right shift of CO oxidation peak with the increase in Pd amount represents the high tolerance of Au-PtPd catalyst for MOR.

Therefore, our study can manifest that Au-PdPt/C is promising candidate as catalyst for DMFC cathode where MOR and ORR occur competitively due to methanol crossover. Although the literature generally agrees that Pd component in PdPt alloy system is unstable in acid media.[24] The objective of this study, however, was not to investigate the degradation mechanism of the alloy electrocatalyst system, but rather to develop high-performance catalyst materials using an Au-PdPt alloy system. In future studies, we will insightfully investigate the stability of Au-PtPd multi metallic system in acid media.

Conclusions

Carbon-supported Au NPs were decorated with Pt, bimetallic PtPd and Pd structures by successive reduction process. HR-TEM, XRD and XPS analyses revealed uniformly distributed fine NPs (< 5 nm in diameter) on carbon particles, and the selectively deposited Pt and bimetallic PtPd, Pd structures on Au surface. The Au-Pt NPs exhibit high electrocatalytic reactivity for ORR in H_2SO_4 solutions without CH_3OH, due to its structural effect. In H_2SO_4 solutions with CH_3OH, the MOR tolerance of Au-PtPd NPs increased as the ratio of Pt decreased, and these represented much higher activity than those of Au-Pt NPs and Pt/C. The more enhanced MOR tolerance of Au-PtPd NPs is ascribed to the synergistic effect resulting from its thin structure and bimetallic PtPd composition.

Experimental

Preparation of the electrocatalysts The carbon-supported 30 wt. % Au (Au/C) NPs were synthesized using $NaBH_4$ and sodium citrate ($Na_3C_6H_5O_7 \cdot 2H_2O$), as described in previous
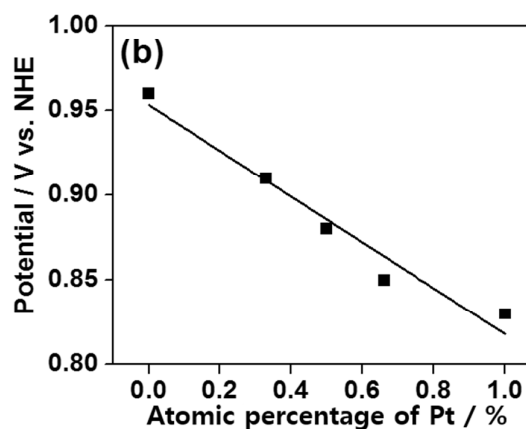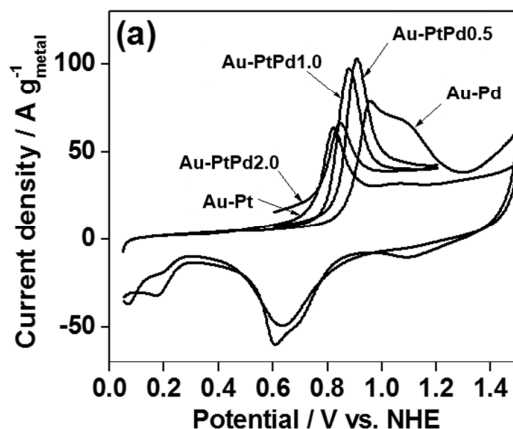
report.[6] The selective deposition of Pt, PtPd and Pd were as follows: Ascorbic acid ($C_6H_8O_6$, 0.26 g) was added to 400 ml of

Fig. 7 (a) CO stripping voltammograms of Au-Pt, Au-PtPd, Au-Pd catalysts in 0.5 M H_2SO_4 at a sweep rate of 20 mVs^{-1} and (b) potential of CO oxidation peak vs. atomic percentage of Pt curve..

the Au/C-dispersed solution at room temperature, and was followed by the addition of adequate amounts of Pt ($H_2PtCl_6 \cdot xH_2O$, Aldrich) and Pd precursor($Pd(NO_3)_2 \cdot xH_2O$), Aldrich). In preparation of Au-Pd NPs, Pd precursor was added at 333 K for its complete reduction. After stirring for 20 h, the resultant solution was filtered, washed and dried in a vacuum oven at 343 K. The total amount of active elements (Pt and Pd) was the same atomic percent as the Au in all samples [(Pt+Pd)/Au=1.0]. The Au-PtPd NPs were designated as Au-PtPdX, where X indicates the atomic ratio of Pt to Pd.

Physical characterization of the electrocatalysts High resolution-transmission electron micrographs (HR-TEM) were obtained on a JEOL 2010 equipped with energy-dispersed X-ray microanalysis (EDX) at 200 kV accelerating voltage. X-ray diffraction (XRD) was carried out with a Rigaku D/MAX 2500 operated with a Cu Kα source (λ= 1.541 Å) operating at 40 kV and 100 mA. X-ray photoelectron spectroscopy (XPS) was performed using an AXIS (KARATOS) photoelectron

ARTICLE

spectrometer and the X-ray source was Mg Kα operating at 15 kV and 150 W.

Electrochemical characterization of the electrocatalystsA cyclic voltammogram (CV) was obtained in a conventional three-electrode electrochemical cell using a glassy carbon (GC) electrode (5 mm diameter) as a working electrode, and Pt wire as a counter electrode, and saturated calomel electrode (SCE) as a reference electrode. Electrochemical experiments were performed in a de-aerated 0.5 M H_2SO_4 solution with a general purpose electrochemical system (Autolab, Eco Chemie). For the preparation of NPs slurry, 500 µl of DI water, 572 µl of 5 wt. % Nafion® solution (Aldrich Chem. Co) and 4 ml of 2-propanol per 0.1 g of prepared NPs powder were mixed, and then stirred to homogeneity. A constant amount of slurry was dropped on the GC electrode with a micropipette. For the measurement of activities for ORR, linear sweep voltammetry was conducted in oxygen-saturated 0.5 M H_2SO_4 and 0.5 M H_2SO_4/0.1 M CH_3OH solutions using rotating disk electrode (RDE). The CVs were recorded from 1.1 to 0.1 V with a scan rate of 5 mV s^{-1} and a rotation speed of 3000 rpm. CO stripping experiments were conducted in 0.5 M H_2SO_4. First, CO was adsorbed on the catalysts while maintaining the potential at 0.1 V for 25 min by bubbling CO gas into the solution. After the adsorption of CO, the CO gas was replaced withAr gas to reduce the remaining CO in the solution while holding the potential at 0.1 V for 30 min. Then, the potential was varied from 0.05 V to 1.5 V at 20 mVs^{-1} to record the CO stripping voltammograms.

Acknowledgements

Notes and references

1   W. Yuan, K. Scott and H. Cheng, *J. Power Sources*, 2006, **163**, 323.
2   H.Q. Li, Q. Xin, W.Z. Li, X.H. Zhou, L.H. Jiang, S.H. Yang and G.Q. Sun, *Chem. Commun.*, 2004, **1**, 2776.
3   D.C. Papageorgopoulos, M. Keijzer, J.B.J. Veldhuis and F.A. de Bruijn, *J. Electrochem. Soc.*, 2002, **149**, A1400.
4   B. Álvarez, V. Climent, A. Rodes and J.M. Feliu, *J. Electroanal. Chem.*, 2001,**497**, 125.
5   H.C. Ye and R.M. Crooks, *J. Am. Chem. Soc.*, 2007, **129**, 3627.
6   I.-S. Park, B. Choi, D.-S. Jung and Y.-E. Sung, *Electrochim. Acta*, 2006, **52**, 1683.
7   I.-S. Park, K.-S. Lee, J.-H. Choi, H.-Y. Park and Y.-E. Sung, *J. Phys. Chem. C*, 2007, **111**, 19126.
8   I.-S. Park, K.-S. Lee, S.-J. Yoo, Y.-H. Cho and Y.-E. Sung, *Electrochim. Acta*, 2010, **55**, 4339.
9   K.-S. Lee, I.-S. Park, H.-Y. Park, T.-Y. Jeon, Y.-H. Cho and Y.-E. Sung, *J. Electrochem. Soc.*, 2009, **156**, B1150.
10 Y.J. Xiong, H.G. Cai, B.J. Wiley, J.G. Wang, M.J. Kim and Y.N. Xia, *J. Am. Chem. Soc.*, 2007,**129**, 3665.
11 S. Panigrahi, S. Basu, S. Praharaj, S. Pande, S. Jana, A. Pal, S.K. Ghosh and T.J. Pal, *Phys. Chem. C*, 2007, **111**, 4596.
12 Y. J. Xiong, B. Lim, S. E. Skrabalak and Y. N. Xia, *Angew. Chem. Int. Ed.*, 2009, **48**, 60.
13 T. Toda, H. Igarashi, H. Uchida and M. Watanabe, *J. Electrochem. Soc.*, 1999,**146**, 3750.
14 L. Liu and E. Pippel, *Angew. Chem. Int. Ed.*, 2011, **50**, 2729.
15 J. Yang, C.H. Cheng, W. Zhou, J.Y. Lee and Z. Liu, *Fuel Cells*, 2010, **10**, 907.
16 X. Li, Q. Huang, Z. Zou, B. Xia and H. Yang, *Electrochim. Acta*, 2008, **53**, 6662.
17 W.M. Wang, D. Zheng, C. Du, Z.Q. Zou, X.Q. Zhang, B.J. Xia, H. Yang and D.L. Akins, *J. Power Sources*, 2007, **167**, 243.
18 K. Lee, O. Savadogo, A. Ishihara, S. Mitsushima, N. Kamiya, K.-I. Ota, *J. Electrochem. Soc.*, 2006, **153**, A20.
19 W.M. Wang, Q.H. Huang, J.Y. Liu, Z.Q. Zou, Z.L. Li and H. Yang, *Electrochem. Commun.*, 2008,**10**, 1396.
20 W. He, J.Y. Liu, Y.J. Qiao, Z.Q. Zou, X.G. Zhang, D.L. Akins and H. Yang, *J. Power Sources*, 2010, **195**, 1046.
21 S. An, J. Park, C. Shin, J. Joo, E. Ramasamy, J. Hwang and J. Lee, *Carbon*, 2001, **49**, 1108.
22 A.N. Golikand, E. Lohrasbi, M.G. Maragheh and M. Asgari, *J. Appl. Electrochem.*,2009, **39**, 2421.
23 I.-S. Park, K.-S. Lee, Y.-H. Cho, H.-Y. Park and Y.-E. Sung, *Catal. Today*, 2008, **132**, 127-131.
24 Y. Liu, M. Chi, V. Mazumder, K.L. More, S. Soled, J.D. Henao and S. Sun, *Chem. Mater.*, 2011, **23**, 4199-4203.